THE JOURNAL OF PHYSICAL CHEMISTRY B

Article

pubs.acs.org/JPCB

Mechanistic and Conformational Flexibility of the Covalent Linkage Formed during β-Lyase Activity on an AP-Site: Application to hOgg1

Jennifer L. Kellie and Stacey D. Wetmore*

Department of Chemistry and Biochemistry, University of Lethbridge, 4401 University Drive West, Lethbridge, Alberta, T1K 3M4, Canada

Supporting Information

ABSTRACT: The β/δ-lyase activity of bifunctional glycosylases on damaged nucleotides in DNA involves the formation of a covalent linkage between the protein (lysine or N-terminal proline) and DNA (C1′ of the damaged nucleotide). In the present study, the conformational and mechanistic flexibility of the cross-link is examined. Repair of 8-oxoguanine damage by hOgg1 is considered as a representative system, and the glycosylase through β-lyase steps are investigated using density functional theory. (PCM/SMD)-M06-2X/6-311+G(2df,2p)//PCM-B3LYP/6-31G(d) energetics were determined for eight unique mechanisms differing in the conformation of the imine linkage (*E*/*Z*), the proton (*pro*−*S*/*R*) abstracted during elimination, and whether the ring-opening step is base catalyzed. This initial study used a model system limited to the damaged nucleoside 3′-monophosphate and a model nucleophile to investigate this series of complex reaction steps. The great flexibility exhibited by the linkage and clustered β-elimination energetics indicate sterics will play a large role in predicting the preferred lyase mechanism for a given enzyme. The stationary points identified herein can be overlaid into a protein structure to assist in generating initial guesses for large model systems. By comparing the characterized geometries and enzyme active sites, methods for catalysis of the various chemical steps can be identified, and these possibilities are discussed in detail for hOgg1. Interestingly, the most stable structure on the potential energy surface occurs *before* elimination of the 3′-phosphate. Hydrolysis of the protein−DNA cross-link at this point would yield an AP-site, which provides support for the recently observed monofunctional activity of hOgg1.

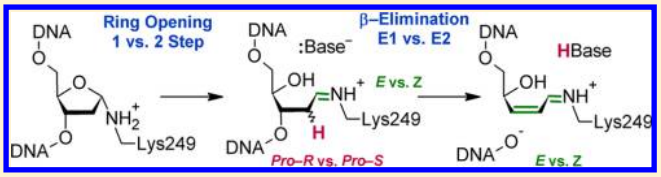

INTRODUCTION

Cleavage of the DNA backbone (for example, β/δ-lyase activity) is an essential step in the repair of damaged nucleotides through the base and nucleotide excision repair pathways.[1] In base excision repair, the DNA backbone may be nicked by an AP-endonuclease after removal of the damaged base by a monofunctional glycosylase, or through the lyase activity of a bifunctional glycosylase. For example, human 8-oxoguanine−DNA glycosylase (hOgg1) catalyzes both deglycosylation (EC#: 3.2.2.−) and β-elimination of the 3′-phosphate (EC#: 4.2.99.18) of the 8-oxoguanine nucleotide (dOG) to yield an apurinic/apyrimidinic site (AP-site) with a nick on the 3′-side (Scheme 1).[2−5] hOgg1 activity is critical because of the high mutagenicity of the OG (nucleobase) lesion, which has a preference for Hoogsteen base-pairing with adenine and thereby leads to G:C → T:A transversion mutations upon replication.[6−8] In addition, OG is a common product of attack on cellular DNA by reactive oxygen species and is formed 10^3 times per cell per day in normal cells.[9−11]

Shortly after the discovery of hOgg1, it was determined that Lys249 is responsible for catalysis and covalently binds to the AP-site.[12] Later studies of the various stages of the hOgg1 mechanism have focused on protein structure and lesion recognition. For example, Verdine et al. have successfully used a combination of protein−DNA cross-linking and borohydride trapping to obtain X-ray crystal structures of hOgg1 (with various mutations) at different stages in the binding and chemical steps.[13−23] In addition to providing support for the role of Lys249,[13] these studies have determined that Asp268 is catalytic in several steps, partially through the stabilization of multiple Schiff base intermediates (Scheme 1).[17,23] Furthermore, the nucleobase generated upon deglycosylation has been found to behave as a cofactor for O3′-elimination, and displays a *pro*−*R*:*pro*−*S* preference for C2′−H abstraction depending on the C8-substituent.[16] Gln315 has been identified to be weakly catalytic and important for substrate binding (and specificity) through hydrogen bonding with the OG nucleobase.[21,24] However, experimental studies show hOgg1 activity on substrates with reduced hydrogen-bonding capabilities,[25,26] which contradicts the proposed catalytic importance of hydrogen bonding and/or proton transfer to the OG nucleobase. Finally, recent evidence indicates that hOgg1 is in fact monofunctional *in vivo*, where Asp268 may play a more prominent role than in the bifunctional mechanism.[23]

Despite the abundance of experimental data and unanswered questions regarding the chemical step implemented by hOgg1, no computational study has examined the complete reaction mechanism of hOgg1 or any other bifunctional glycosylase.

Received: June 27, 2012
Revised: August 1, 2012
Published: August 9, 2012

dx.doi.org/10.1021/jp306344g | J. Phys. Chem. B 2012, 116, 10786−10797

Scheme 1. General Steps in the Commonly Accepted hOgg1 Glycosylase/β-Lyase Mechanism,[16] Including (a) Deglycosylation via Nucleophilic Attack by Lys249,(b) Ring-Opening through Direct or Base-Assisted Transfer of a Proton from the Amine Group, (c) β-Elimination of the 3′-Phosphate with Abstraction of a C2′-Proton, and (d) Hydrolysis of the Schiff Base to Generate a Nicked Product and Release the Enzyme

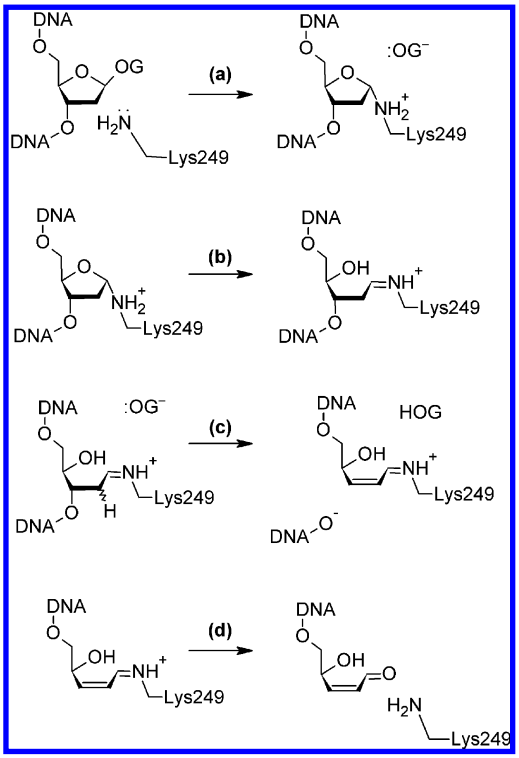

Indeed, previous computational analyses of hOgg1 have focused on the deglycosylation step,[27−31] with a select few considering ring-opening (Scheme 1a,b).[27,29] Furthermore, a thorough computational analysis of the β-elimination of a cross-linked AP-site has yet to be performed. Nevertheless, a few relevant examples can be found in the literature such as the α,β-elimination reactions of esters,[32] or the mechanism of action of phosphothreonine lyase (EC#: 4.2.3.−).[33] However, none of these examples involve a positively charged imine linkage and thus they exhibit different electrostatics at the reaction center than the mechanism catalyzed by hOgg1 and other bifunctional glycosylases. The inherent flexibility of the bifunctional glycosylase reaction explains the absence of literature on the subject. For example, transfer of either proton from the Lys249 terminal amine to O4′ during ring-opening yields different stereoisomers at the imine linkage (*E* and *Z* for *pro*−*S* and *pro*−*R* protons, respectively). In addition, abstraction of either C2′−H leads to different stereoisomers at the C2′−C3′ double bond in the lyase product (*Z* and *E* for *pro*−*S* and *pro*−*R* abstraction, respectively), and this isomeric information is lost upon crystallization of the intermediates due to reduction of the unsaturated bonds in the protein−DNA cross-link.[16] Therefore, there is a clear need for computer modeling of these flexible reactions, which will provide structural information that is difficult to obtain from experiments.

Since few lyases have been studied as extensively (and crystallized in as many different stages of the reaction) as hOgg1, this enzyme is an excellent candidate for investigating the complicated β-lyase reaction. The present work characterizes eight unique chemically relevant pathways relevant to hOgg1 and other bifunctional glycosylases, which can use more than one mechanism (for example, lyase activity of hOgg1 has been shown to proceed with abstraction of either C2′−H proton).[16] The mechanisms consider the conformational and mechanistic flexibility of the different isomers of the imine linkage (Scheme 1), the effect of transfer of either amino proton during the ring-opening step (Scheme 1b), and *pro*−*R* versus *pro*−*S* proton abstraction from C2′ during the β-lyase step (Scheme 1c). As a consequence of the complexity and number of reaction mechanisms considered, density functional theory (DFT) and a small computational model are used. Nevertheless, our results provide insight into the degree of movement required to form the different isomers of the covalent linkage throughout the mechanism. Indeed, small model studies are essential to our understanding of the mechanistic intricacies before undertaking large-scale enzymatic modeling and help ensure that all sterically relevant mechanisms are considered. To this end, this work will propose the most appropriate mechanisms for future large-scale modeling of hOgg1 and describe a method of incorporating these results into an enzyme active site. Furthermore, possible methods for catalysis of OG excision by hOgg1 will be identified by analyzing the barriers inherent to the glycosylase and β-lyase mechanisms. Finally, the results of this study will be discussed with respect to the possible monofunctional (glycosylase only) activity of hOgg1.[23] Although we focus on applying these results to one enzyme, the data within can be used for similar analyses of other systems with β-lyase activity (EC# 4.2.99.18), such as FPG,[34] endonuclease III,[35] endonuclease VIII,[36] and MutY (EC#: 3.2.2.−, which exhibits weak, uncoupled lyase ability),[37] as well as model peptides (for example, Lys-Trp-Lys).[38]

COMPUTATIONAL DETAILS

In the present study, the flexibility of the imine linkage formed during β-lyase activity was examined using the repair of dOG by hOgg1 as a representative system, a diverse collection of mechanisms, and a DFT model. First, the mechanisms investigated will be summarized, and the model implemented will be described. In the Results section, the DFT structures and energetics will be presented for all mechanisms, including detailed potential energy surfaces (PES) of the elimination phase for select mechanisms. The Discussion section will subsequently outline broad biochemical implications of the results, propose possible methods for catalysis of β-elimination, and explain the potential monofunctional activity of hOgg1.

Mechanisms and Model. The main phases in the overall chemical reaction catalyzed by hOgg1 are outlined in Scheme 1. In the first phase (a), S_N2 deglycosylation of the damaged nucleotide produces a free OG^- nucleobase anion and an AP-site covalently bound to hOgg1 through the terminal amine of Lys249.[12] Although there has been some discussion of a possible S_N1 mechanism for hOgg1,[17,18,20,28,39] there is little experimental evidence to support such a statement. Indeed, these conclusions appear to be based on uracil−DNA glycosylase (EC#: 3.2.2.3), a monofunctional enzyme that shifts the pK_a of uracil by 3.4 units through a strong hydrogen bond with His268 to promote base departure.[40] No equivalent strong hydrogen bond with OG is observed in the hOgg1 active site.[13] In the second phase of the hOgg1 chemical step, the amine linkage rearranges to a Schiff base through transfer of a

dx.doi.org/10.1021/jp306344g | J. Phys. Chem. B 2012, 116, 10786−10797

proton from Nε to O4′ of the deoxyribose ring, causing the ring to open (b).[16,41] The third phase (c) involves β-elimination of the 3′-phosphate group with abstraction of a proton from C2′. There is evidence that either the *pro*−*R* or *pro*−*S* proton (C2′−H_R and C2′−H_S) can be removed during hOgg1 activity.[16] The final phase (d) involves hydrolysis of the imine linkage to regenerate the enzyme and release the final product. In the present study, eight mechanisms were fully characterized for phases **a**−**c**. Consistent with Scheme 1, the nomenclature for stationary points referring to deglycosylation will end in (a), those referring to the ring-opening step(s) will end in (b), and those corresponding to the elimination steps will end in (c); for example, the transition state for deglycosylation and succeeding intermediates are denoted as TS(a) and IC(a), respectively. Additional stationary points characterized for phases with more than one step are identified with a prime; for example, the intermediate between C2′−H abstraction and O3′-elimination is labeled IC(c′).

Table 1 summarizes the eight mechanisms considered. Deglycosylation (a) occurs via the same S_N2 pathway in all cases. Ring-opening (b) was modeled as either direct (D) or OG-assisted (A), and involves transfer of either the *pro*−*R* (N_R) or *pro*−*S* (N_S) proton on Nε. A stepwise elimination (c) initiated by abstraction of either the *pro*−*R* (C_R) or the *pro*−*S* (C_S) proton on C2′ was characterized for all pathways. Thus, the nomenclature for each reaction pathway specifies the aspects of the phases (b) and (c) that differ across the mechanisms. For example, the D-N_RC_R mechanism denotes direct transfer of Nε−H_R to O4′ in phase (b) and abstraction of C2′−H_R in phase (c).

Table 1. Nomenclature for the Glycosylase/β-Lyase Mechanisms Investigated in the Present Work[a]

mechanism	ring-opening	Nε−H[b]	C2′−H[c]
D-N_RC_R	direct	*pro*−*R*	*pro*−*R*
D-N_RC_S	direct	*pro*−*R*	*pro*−*S*
D-N_SC_R	direct	*pro*−*S*	*pro*−*R*
D-N_SC_S	direct	*pro*−*S*	*pro*−*S*
A-N_RC_R	assisted	*pro*−*R*	*pro*−*R*
A-N_RC_S	assisted	*pro*−*R*	*pro*−*S*
A-N_SC_R	assisted	*pro*−*S*	*pro*−*R*
A-N_SC_S	assisted	*pro*−*S*	*pro*−*S*

[a]See Figure 1 for atom numbering. [b]Proton transferred from the amine to O4′ during ring-opening. [c]Proton abstracted from C2′ during the elimination step.

The smallest model capable of the reactions highlighted in phases a−c in Scheme 1 was used. Specifically, for the glycosylase/β-lyase chemical steps catalyzed by hOgg1, this includes the OG nucleoside, 3′-phosphate, and lysine nucleophile (Figure 1). Several previous computational investigations of OG deglycosylation have used models of similar size but without the phosphate group.[27,28,30,31] Within our model, the OG nucleobase acts as the general base or general acid required at various stages in the mechanism, which eliminates the requirement of additional groups and model expansion. Although this approach allows the model to be consistent throughout the entire reaction pathway, the alignment of the OG nucleobase deviates from an orientation that would "fit" in the hOgg1 active site at some stages of the mechanisms. Nevertheless, our primary goal and overall findings regarding the reactivity and flexibility of the imine linkage are unaffected by this computational artifact.

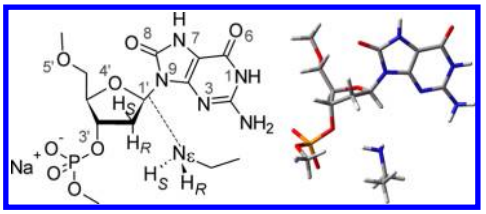

Figure 1. 2D (left) and 3D (right) representations of the computational model used in the present study, which contains 8-oxoguanosine 3′-monophosphate, ethyl amine (lysine), and a sodium counterion. Atomic numbering shown in gray, including *pro*−*R* and *pro*−*S* notation for hydrogen atoms involved in the abstraction steps.

The truncation points of the DNA phosphate backbone (terminal oxygen atoms) were capped with methyl groups to prevent hydrogen-bonding interactions that are unfeasible in an extended system. The charge on the phosphate group was balanced with a sodium counterion, since this method yields better nucleotide geometries than other (protonated or anionic) models.[42,43] The side chain of the nucleophilic lysine was modeled as ethyl amine, since preliminary results show that the structure or energetics of the first (deglycosylation) barrier is unaffected by further extension of the amine. Although debates exist in the literature regarding the initial charge of the nucleophile and the potential mode of activation,[23,29] the lysine residue must be neutral to initiate repair. The neutral lysine used in the present work is supported by proposals that Lys249 may be activated during substrate binding,[15] and speculations from mutational studies that the pK_a of Lys249 in the hOgg1 active site may be shifted such that a significant percentage of the population is neutral.[17] Therefore, the nucleophile activation step (if required) would occur before the reactions investigated herein. Previous theoretical studies have activated the nucleophile by transferring a proton to the OG nucleobase,[27−29] which is consistent with the general observation that purine deglycosylation requires leaving group activation.[4,44] However, protonation of 8oxoG would diminish the ability of the nucleobase to act as a general base in later steps of the reaction, which is required by our model.

Methodology. The initial geometry of the OG nucleotide was taken from the 1EBM crystal structure of hOgg1 bound to OG-containing DNA[8] to account for changes in the sugar−phosphate backbone upon flipping the nucleotide out of the helix and into the active site. Subsequently, a sodium counterion was added equidistant to the two phosphate oxygen atoms and a model lysine was positioned for S_N2 attack. Fully optimized geometries were obtained using B3LYP/6-31G(d) in the presence of bulk solvent described by the IEF-PCM method implemented in Gaussian 09.[45] A dielectric constant of 4.24 (diethyl ether) was selected to represent the environment inside the active site.[46] Frequency calculations at the same level of theory were used to verify the nature of stationary points and obtain zero-point vibrational and Gibbs corrections. All stationary points were reoptimized with PCM-B3LYP/6-31+G(d) to determine the possible influence of diffuse functions on the reaction. The resulting structural changes are minor, and the calculated reaction energetics are unchanged (see the Supporting Information).

Reaction potential energy surfaces were generated for select mechanisms (see Results) to assist in characterizing the E2 and O3′-elimination transition states. The ring-opened intermediate

Table 2. Relative Energies (kJ mol^{-1}) for Stationary Points Characterized along the Eight Glycosylase/β-Lyase Mechanisms[a]

	D-N_RC_R	D-N_SC_R	D-N_RC_S	D-N_SC_S	A-N_RC_R	A-N_SC_R	A-N_RC_S	A-N_SC_S
				ΔE^b				
TS(a)	147.4	147.4	147.4	147.4	147.4	147.4	147.4	147.4
IC(a)	64.0	64.1	60.6	64.1	−5.6	5.8	−5.6	5.8
TS(b)	201.2	190.5	201.2	190.5	−15.8	−2.0	−15.8	−2.0
IC(b′)					−10.0	−15.1	−10.0	−22.7
TS(b′)					48.2	55.9	48.2	55.9
IC(b)	34.3	29.3	85.4	75.9	49.1	55.2	43.4	43.4
TS(c)	94.8	83.3	96.1	96.8	81.3	89.9	72.5	72.5
IC(c′)	64.4	22.7	58.4	72.5	55.0	58.0	53.0	52.9
TS(c′)	157.3	107.2	170.1	168.9	154.0	181.1	185.7	185.7
IC(c)	155.6	21.4	98.2	92.6	57.0	140.0	48.3	48.3
				ΔG^c				
TS(a)	147.4	147.4	147.4	147.4	147.4	147.4	147.4	147.4
IC(a)	59.6	59.6	53.0	59.6	−6.6	9.8	−6.6	9.8
TS(b)	199.8	189.6	199.8	189.6	−15.4	2.4	−15.4	2.3
IC(b′)					−12.5	−12.9	−12.5	−22.2
TS(b′)					49.5	64.2	50.7	64.2
IC(b)	36.0	27.6	77.4	71.1	48.1	57.8	41.2	41.2
TS(c)	90.2	81.9	95.1	95.7	83.3	90.6	74.1	74.1
IC(c′)	59.0	15.0	51.6	68.1	53.2	55.4	53.3	53.3
TS(c′)	136.2	100.3	158.9	156.0	150.3	170.0	176.3	176.3
IC(c)	128.6	7.4	75.5	70.1	44.2	128.7	20.5	20.5

[a]Energies reported relative to a common reactant complex (Figure 1). [b]PCM-M06-2X/6-311+G(2df,2p)//PCM-B3LYP/6-31G(d) values including scaled (0.9806) zero-point vibrational energy correction. [c]SMD-M06-2X/6-311+G(2df,2p)//PCM-B3LYP/6-31G(d) values including unscaled correction to Gibbs energy.

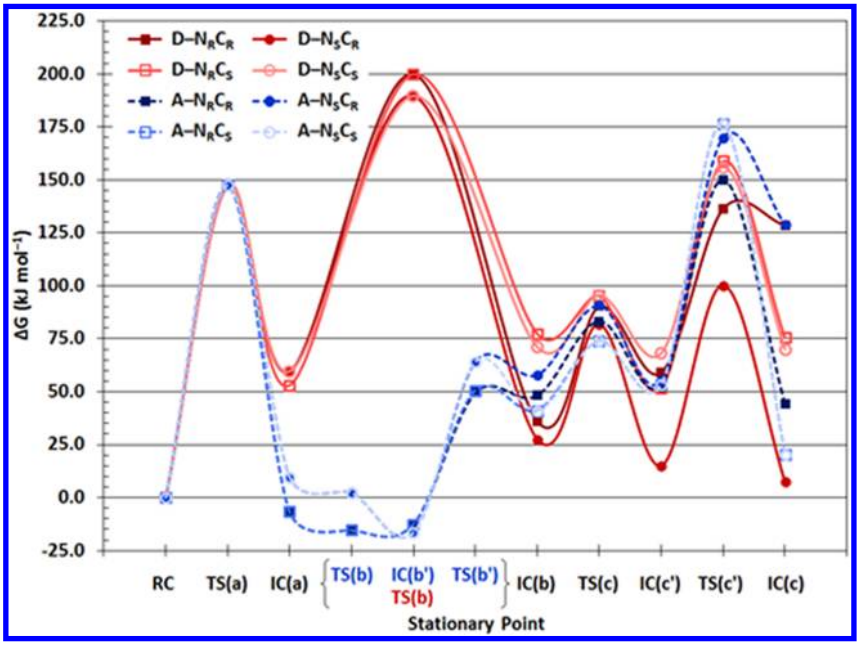

Figure 2. SMD-M06-2X/6-311+G(2df,2p)//PCM-B3LYP/6-31G(d) Gibbs relative energies (kJ mol^{-1}) along the eight glycosylase/β-lyase mechanisms considered in the present work, which involve direct (solid red line) or assisted (dashed blue line) ring-opening, transfer of the Nε−H_R (square) or Nε−H_S (circle) proton, and abstraction of the C2′−H_R (filled) or C2′−H_S (empty) proton.

(IC(b), Scheme 1) was used as a starting point for these surfaces. The (C2′−H or C3′−O3′) bonds being broken defined the reaction coordinates and were altered in a stepwise manner by increments of 0.100 Å (C2′−H) or 0.200 Å (C3′−O3′) to generate the elimination surface. The stationary points identified from the surfaces were then relaxed to yield fully optimized structures for the representative mechanisms and provide guesses for the remaining mechanisms.

The connection between intermediates and adjacent transition states for phases (a) and (b) were verified through intrinsic reaction coordinate (IRC) calculations and through inspection. The connection between stationary points for phase (c) was verified by the reaction PES. Intermediates obtained through forward (from the preceding TS) and reverse (from the succeeding TS) IRCs are related by low barrier rotations. Efforts were made to characterize the rotational transition

dx.doi.org/10.1021/jp306344g | J. Phys. Chem. B 2012, 116, 10786−10797

states, but stable structures could not be found. Regardless, the motion is always associated with the nucleobase, which is a representative acid/base in the current model, and therefore, the main conclusions of this study will be unaffected. Thus, the lowest energy minimum was selected to represent a given intermediate in each mechanism. Single-point calculations were carried out with M06-2X/6-311+G(2df,2p), since M06-2X performs well for S_N2 and E2/E1 reaction energetics.[47] The Gibbs energy was determined by combining the B3LYP Gibbs energy correction with the M06-2X/6-311+G(2df,2p) single-point energy calculated using the SMD solvation method, which includes the nonelectrostatic component of the energy. This approach has recently been reported to yield reliable Gibbs energies.[48]

All calculations were carried out with Gaussian 09.[49]

RESULTS

The energetics for the eight reaction mechanisms are presented in Table 2, and the SMD-M06-2X/6-311+G(2df,2p) Gibbs reaction surfaces are shown in Figure 2. Unless otherwise specified, all energies in the text refer to the Gibbs surface. Each aspect of the overall mechanism is discussed in detail below.

Deglycosylation. All mechanisms share a common reactant (Figure 1) and concerted deglycosylation transition state (TS(a), Figure 3). In the reactant, the OG nucleotide is in an *anti* conformation about the glycosidic bond, and the deoxyribose ring adopts a C3′-*exo* pucker with a slight C2′-*endo* twist. The model lysine is positioned on the opposite side of the sugar moiety than the nucleobase, and is involved in a weak hydrogen bond to O3′. The transition state contains a glycosidic bond length of 2.441 Å and a C1′−Nε distance of 2.381 Å, and therefore is slightly earlier than the TS reported in our previous gas-phase study (d(C1′−N9) = 2.552 Å and d(C1′−Nε) = 2.014 Å),[31] and other theoretical studies.[28,29] The barrier to deglycosylation is 147.4 kJ mol^{-1} on both the ΔE and ΔG surfaces. Thus, the 3′-phosphate group lowers the calculated S_N2 barrier compared to a truncated (nucleoside) model with a neutral lysine nucleophile (186.2 kJ mol^{-1} as determined using B3LYP/6-31+G(d)).[28]

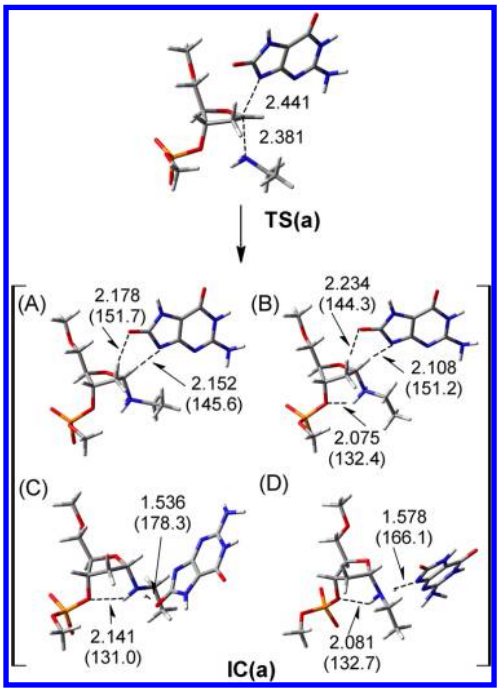

Figure 3. Structures along the deglycosylation step for all mechanisms: (A) D-N_RC_R, D-N_SC_R, and D-N_SC_S; (B) D-N_RC_S; (C) A-N_RC_R and A-N_RC_S; (D) A-N_SC_R and A-N_SC_S. Important PCM-B3LYP/6-31G(d) distances (Å) and angles (deg, in parentheses) provided (sodium counterion omitted for clarity). Mechanism nomenclature and reaction energetics can be found in Tables 1 and 2, respectively.

Following cleavage of the glycosidic bond, the PES divides into direct and base-assisted ring-opening mechanisms. Consequently, the deglycosylation TS falls to one of four deglycosylated intermediates (IC(a), Figure 3). The intermediates on the direct ring-opening surfaces contain a weak contact between O8 in OG and C2′−H_S (Figure 3A,B). In contrast, the assisted ring-opening intermediates contain strong hydrogen bonds between one of the amine hydrogen atoms and either O8 (Figure 3C, A-$N_RC_{R/S}$) or N9 (Figure 3D, A-$N_SC_{R/S}$) of the nucleobase. As a result, the assisted ring-opening intermediates are significantly more stable than those for direct transfer (by 43.2−66.4 kJ mol^{-1}, Table 2). Since the eight mechanisms diverge after the deglycosylation step, the pathways involving direct ring-opening will first be discussed, followed by the base-assisted ring-opening mechanisms.

Direct Ring-Opening: Nε−$H_{R/S}$ Transfer. The structures for the mechanisms involving direct proton-transfer of Nε−H_R to O4′ are shown in Figure 4. Significant rotation about the cross-link is required to allow for transfer of the *pro*−*R* proton. The corresponding transition state (TS(b)) has a ΔG value of 199.8 kJ mol^{-1} relative to the reactant ($\Delta G^{\ddagger}$ = 140.2 kJ mol^{-1}). This common transition state falls to a distinct IC(b) geometry for each of the D-N_RC_R and D-N_RC_S mechanisms with relative Gibbs energies of 36.0 and 77.4 kJ mol^{-1}, respectively. In addition, D-N_RC_R IC(b) (Figure 4, left) contains hydrogen-bonding interactions between the OG nucleobase and C1′−H and Nε−H, while D-N_RC_S IC(b) (Figure 4, right) contains a single C2′−H_S···O8 interaction.

In contrast to transfer of the *pro*−*R* proton, rotation of lysine is unnecessary for direct transfer of the *pro*−*S* Nε−H (Figure 5). Ring-opening occurs with a Gibbs energy of 189.6 kJ mol^{-1} relative to the reactant, which is only slightly lower (by 10.2 kJ mol^{-1}) than the *pro*−*R* proton transfer energy (Table 2). Proton transfer of the *pro*−*S* hydrogen leads to *E*-isomer intermediates (IC(b)) with similar structures to the *Z*-isomers characterized for D-$N_RC_{R/S}$. The largest difference in stability (6 kJ mol^{-1}) occurs for the D-N_SC_R ring-opened intermediate, since the hydrogen-bond acceptors are reversed compared to the corresponding D-N_RC_R intermediate, and therefore D-N_SC_R contains a strong (1.504 Å) Nε−H···O8 hydrogen bond and a weak (2.291 Å) C2′−H_R···N9 contact. Attempts to characterize a structure similar to D-N_RC_R IC(b) that is connected to an elimination product were unsuccessful.

Direct Ring-Opening: β-Elimination. Subsequent to ring-opening, abstraction of a proton from C2′ initiates elimination of O3′. The OG contact with C2′−H_S in the D-N_RC_S ring-opened intermediate (Figure 4) reduces the barrier for abstraction to ∼18 kJ mol^{-1} compared to a barrier of ∼54 kJ mol^{-1} for *pro*−*R* abstraction (Table 2). The elimination intermediate IC(c′) is more stable for *pro*−*S* abstraction than for *pro*−*R* abstraction, which is in agreement with the lower TS(c) barrier. Following proton transfer, the O3′-elimination transition states (TS(c′)) and intermediates (IC(c)) are partially stabilized by a tight hydrogen bond (1.521−1.670 Å, Figure 4) between the new O4′-hydroxyl group and a

dx.doi.org/10.1021/jp306344g | J. Phys. Chem. B 2012, 116, 10786−10797

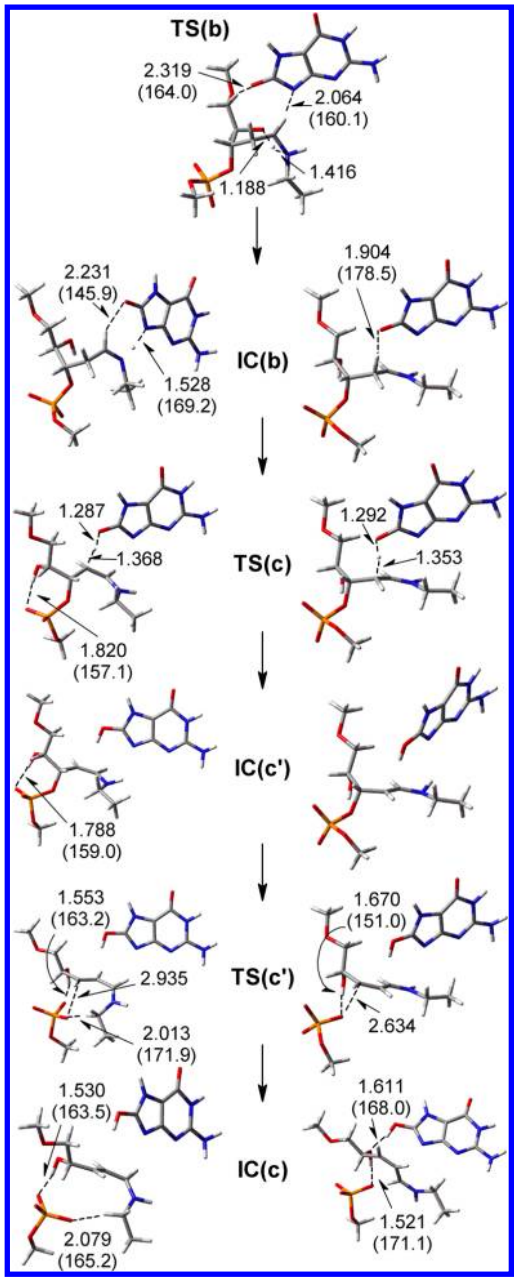

Figure 4. Structures along the ring-opening and β-elimination steps of the D-N_RC_R (left) and D-N_RC_S (right) mechanisms. Important PCM-B3LYP/6-31G(d) distances (Å) and angles (deg, in parentheses) provided (sodium counterion omitted for clarity). Mechanism nomenclature and reaction energetics can be found in Tables 1 and 2, respectively.

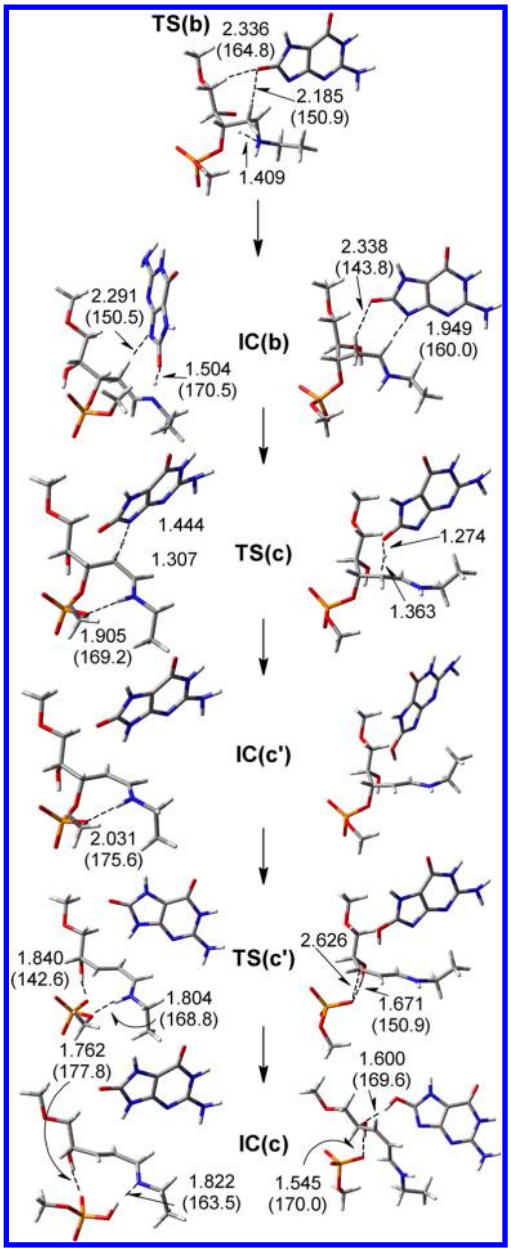

Figure 5. Structures along the ring-opening and β-elimination steps of the D-N_SC_R (left) and D-N_SC_S (right) mechanisms. Important PCM-B3LYP/6-31G(d) distances (Å) and angles (deg, in parentheses) provided (sodium counterion omitted for clarity). Mechanism nomenclature and reaction energetics can be found in Tables 1 and 2, respectively.

phosphate oxygen atom. This additional stabilization is required, since the positively charged imine is directed away from O3′ due to the *Z*-conformation about the C1′−Nε linkage. As a result, a significant barrier (77.2 kJ mol^{-1} for D-N_RC_R and 107.3 kJ mol^{-1} for D-N_RC_S) must be overcome to eliminate the phosphate. Furthermore, the elimination products (IC(c)) are endothermic (by 128.6 and 75.5 kJ mol^{-1} relative to the reactant for D-N_RC_R and D-N_RC_S, respectively). Therefore, these reaction paths are improbable, especially in comparison to others examined in the present work (see below).

The structures and energetics characterized for the elimination pathways of the D-$N_SC_{R/S}$ mechanisms (Figure 5, Table 2) are similar to those for the respective D-$N_RC_{R/S}$ mechanisms. The only exception occurs for D-N_SC_R O3′-elimination. Specifically, in the D-N_SC_R mechanism, the *Z*-conformation about the C1′−C2′ double bond and the pseudo *Z*-conformation about C1′−Nε in the intermediate (IC(c′)) place the imine hydrogen in close proximity to the terminal oxygen of the phosphate group (d(Nε−H···O_{me}) = 2.031 Å). This additional stability, coupled with the O4′−H···O_P interaction observed in the other mechanisms, yields an O3′-elimination barrier of 85.3 kJ mol^{-1}, and produces the most stable IC(c) characterized for all mechanisms when the remaining Nε−H is transferred to O3′ (ΔG = 7.4 kJ mol^{-1} relative to the reactant).

dx.doi.org/10.1021/jp306344g | J. Phys. Chem. B 2012, 116, 10786−10797

Assisted Ring-Opening: Nε−H$_{R/S}$ Transfer. From the summary of direct mechanisms in Figure 2 (red), it can be seen that catalysis of the high energy ring-opening is necessary. Indeed, catalysis by a general base (modeled as the OG nucleobase anion, Figure 6) significantly changes the reaction energetics (Figure 2, blue). Along the base-assisted pathway, proton abstraction from lysine is barrierless (once zero-point vibrational and thermal corrections are included), and leads to exothermic IC(b′) intermediates (ΔG ranging from −22.2 to −12.5 kJ mol^{-1}, Table 2). The corresponding barriers for subsequent ring-opening (TS(b′)) fall between 60 and 90 kJ mol^{-1}, and are significantly lower than the direct ring-opening barriers (>130 kJ mol^{-1}). The proton transfer in the A-N$_R$C$_{R/S}$ mechanisms is facilitated by O8 of OG (Figure 6A), while transfer involves N9 in the A-N$_S$C$_{R/S}$ mechanisms (Figure 6B). The location of the OG nucleobase in TS(b′) of the A-N$_R$C$_{R/S}$ mechanisms is stabilized by a weak (2.137 Å) C1′−H···N9 interaction (Figure 6A) but exhibits significant motion throughout the ring-opening step in A-N$_S$C$_{R/S}$ due to the involvement of N9 in the proton transfer (Figure 6B).

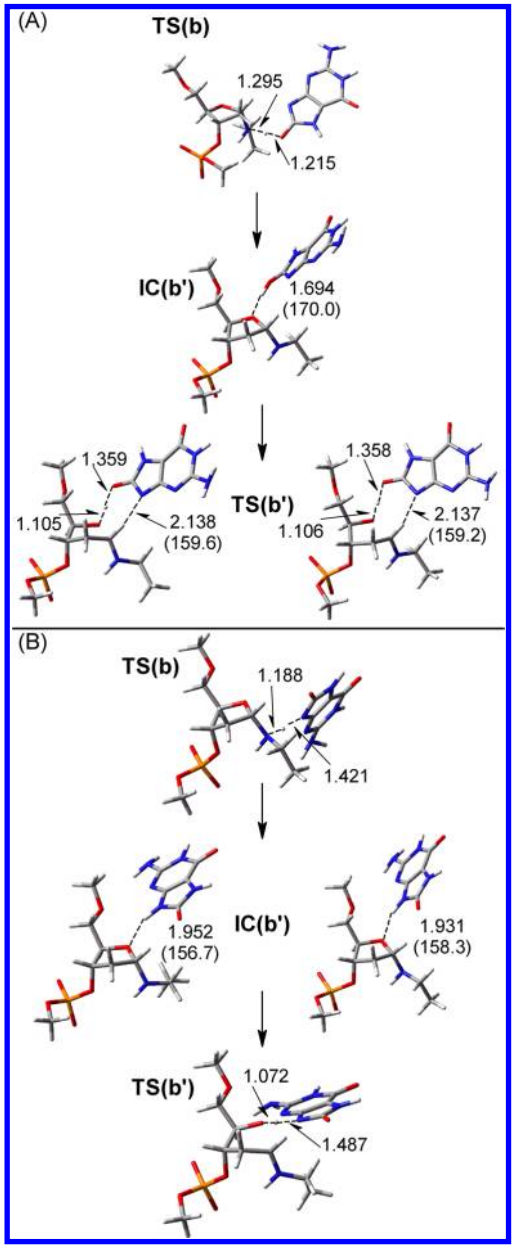

Figure 6. Structures along the ring-opening step of the A-N$_R$C$_R$ (A, left), A-N$_R$C$_S$ (A, right), A-N$_S$C$_R$ (B, left), and A-N$_S$C$_S$ (B, right) mechanisms. Important PCM-B3LYP/6-31G(d) distances (Å) and angles (deg, in parentheses) provided (sodium counterion omitted for clarity). Mechanism nomenclature and reaction energetics can be found in Tables 1 and 2, respectively.

Assisted Ring-Opening: β-Elimination. As observed for the direct mechanisms, the elimination phase corresponding to the assisted ring-opening mechanisms is a two-step process (Figure 7), involving C2′−H abstraction and then O3′-elimination. Throughout all four mechanisms, there is a strong O4′−H···N9 hydrogen bond ranging in length from 1.615 Å (A-N$_S$C$_R$ IC(b)) to 1.967 Å (A-N$_S$C$_R$ IC(c′)), with an average length of 1.87 Å. All four mechanisms have similar barriers for C2′−H abstraction ($\Delta G^{\ddagger} \approx 34$ kJ mol^{-1}) and similarly stable IC(c′) intermediates (53.2−55.4 kJ mol^{-1} relative to the reactant, Table 2). Since N9 forms a strong hydrogen bond with the 4′-hydroxyl, proton transfer occurs to O8 of OG. In addition, the O4′−H···O3′ interaction observed in the direct ring-opening mechanisms is impossible, which therefore increases the O3′-elimination barriers. The only exception occurs for the A-N$_R$C$_R$ mechanism in which the imine linkage is oriented to promote an Nε−H···O interaction that stabilizes the phosphate leaving group (Figure 7A). Since the A-N$_R$C$_R$ mechanism contains additional leaving group stabilization compared to the remaining mechanisms, the O3′-elimination barrier ($\Delta G^{\ddagger}$ = 97.1 kJ mol^{-1}) is lower than the barriers for the other assisted mechanisms (114.6 and 123.0 kJ mol^{-1} for the A-N$_S$C$_R$ and A-N$_{R/S}$C$_S$ mechanisms, respectively (Table 2)). Despite the large barriers, the A-N$_{R/S}$C$_S$ mechanisms lead to the second most stable elimination product (IC(c)). This increased stability is due to a rotation about the C1′−C2′ bond, which allows proton transfer from Nε to O3′ (d(O3′−H···Nε) = 1.859 Å, Figure 7C). While a similar proton transfer occurs along the A-N$_R$C$_R$ mechanism (IC(c), Figure 7A), the phosphate group adopts an inherently less stable orientation.

β-Elimination: E1 versus E2 Pathway. In the mechanisms discussed above, the β-elimination step (Scheme 1c) occurs through an E1 pathway with abstraction of a C2′−H by OG before dissociation of the 3′-phosphate group. Despite our best efforts, and perfect alignment of the β-elimination angle (O3′−C3′−C2′−H$_{R/S}$), transition states corresponding to E2 mechanisms could not be characterized. To verify that the E1 mechanism is the lowest energy pathway, the reaction potential energy surfaces for the D-N$_S$C$_S$ and A-N$_R$C$_R$ mechanisms were characterized, since these selections cover the three main points of variation among all reaction pathways (i.e., direct or assisted ring-opening, Nε−H$_{R/S}$ transfer, and C2′−H$_{R/S}$ abstraction).

The reaction PES (at the optimization level of theory) are shown in Figure 8, where IC(b) falls in the bottom left corner and IC(c) in the top right corner. Therefore, the possible IC(c′) for an E1 mechanism appears near the upper left corner of the surfaces. The surfaces reveal that abstraction of a proton occurs early (d(C2′···H) = 1.400 Å) in the E1 reaction and with a low barrier ($\Delta E^{\ddagger}$ = 16.1 and 19.3 kJ mol^{-1} for D-N$_S$C$_S$ and A-N$_R$C$_R$, respectively). A corresponding exothermic intermediate is found on both surfaces (ΔE = −12.8 and −7.8 kJ mol^{-1} compared to IC(b) for D-N$_S$C$_S$ and A-N$_R$C$_R$, respectively). A dissociative transition state is found at C3′−O3′ distances of 2.700 Å for the direct and 2.500 Å for the assisted ring-opening mechanisms. Consistent with TS(c′) characterized for the relaxed potential energy surfaces (Figure 5), the 4′-hydroxyl

dx.doi.org/10.1021/jp306344g | J. Phys. Chem. B 2012, 116, 10786−10797

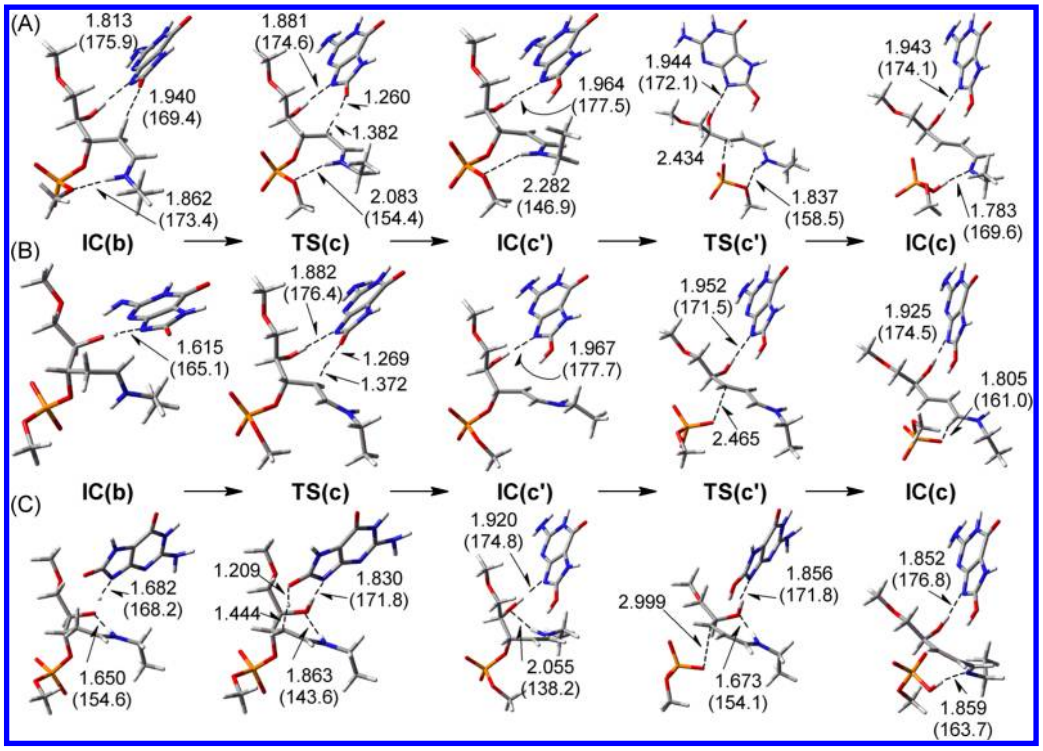

Figure 7. Structures along the β-elimination step of the (A) A-N_RC_R, (B) A-N_SC_R, (C) A-N_RC_S and A-N_SC_S mechanisms. Important PCM-B3LYP/6-31G(d) distances (Å) and angles (deg, in parentheses) provided (sodium counterion omitted for clarity). Mechanism nomenclature and reaction energetics can be found in Tables 1 and 2, respectively.

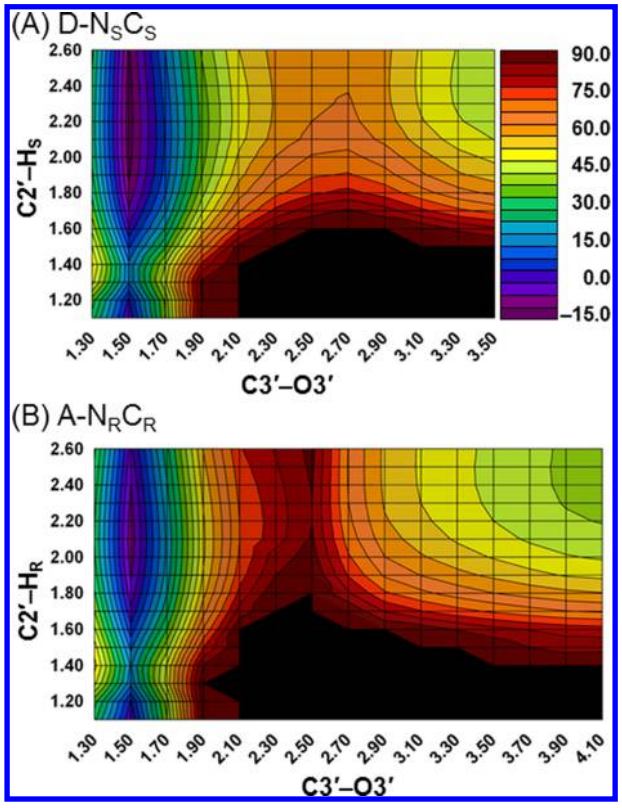

Figure 8. PCM-B3LYP/6-31G(d) reaction potential energy surfaces for the elimination step of the D-N_SC_S (A) and A-N_RC_R (B) mechanisms (see Table 1 for nomenclature). The energies (ΔE, kJ mol^{-1}) are reported relative to the respective ring-opened intermediate (IC(b)) with constrained reaction coordinates.

group stabilizes the phosphate group in the D-N_SC_S mechanism, and thus lowers the barrier compared to A-N_RC_R. In contrast to the E1 pathway, an E2 transition state is ill-defined on both surfaces. Indeed, the synchronous regions of the potential energy surfaces (d(C2′···H) = 1.400, d(C3′···O3′) = 2.300−2.700 Å) are significantly higher in energy than the stepwise regions (>130 kJ mol^{-1} relative to the IC(b) starting point). Since the starting structures were properly aligned for synchronous elimination (β-angle (O3′−C3′−C2′−$H_{R/S}$) ≈ 179°), the large energy difference between the two pathways (E1 versus E2) is likely due to stabilization of proton abstraction by the adjacent Schiff base moiety. Thus, the reaction surfaces clearly support the E1 mechanism reported in the present study. Nevertheless, an E2 pathway may be stabilized within the active site of an enzyme.

■ DISCUSSION

Previous computational investigations of bifunctional glycosylases such as hOgg1 have focused on the deglycosylation step common to all glycosylases[27−31] but have essentially neglected the lyase step. In fact, no computational study has been carried out on the β-elimination of a cross-linked AP-site. As the first step to understanding this challenging process, the core reaction catalyzed by hOgg1 was investigated with a DFT model. Although our model uses the OG nucleobase in the place of possible active-site acids/bases, the results can be extrapolated to other moieties acting in this capacity, and therefore to hOgg1 and other enzymes. In the present study, eight different reaction mechanisms were characterized that span the chemical step catalyzed by bifunctional glycosylases up to enzyme regeneration (Table 1 and Scheme 1). This computational approach yields insight into the types of active-site residues that can contribute to the overall chemical

dx.doi.org/10.1021/jp306344g | J. Phys. Chem. B 2012, 116, 10786−10797

reaction facilitated by hOgg1 and other β-lyases. To this end, each phase of the reaction (Scheme 1) will be discussed separately, as well as the recently recognized monofunctional capability of hOgg1.[23]

Deglycosylation. The first chemical step facilitated by bifunctional glycosylases is cleavage of the glycosidic bond in the damaged nucleotide. Consistent with previous computational studies,[28,29,31] the barrier to deglycosylation of the OG nucleotide was found to be large ($\Delta G^{\ddagger}$ = 147.4 kJ mol^{-1}), and rate-limiting if ring-opening is base catalyzed (Table 2). Since experiment has shown that the lyase step is rate-limiting,[25,50] hOgg1 must significantly reduce the deglycosylation barrier, which is consistent with the catalytic function of other glycosylases.[40,51]

Analysis of the hOgg1 active site (Figure 9) reveals different possible methods to reduce the depurination barrier for dOG

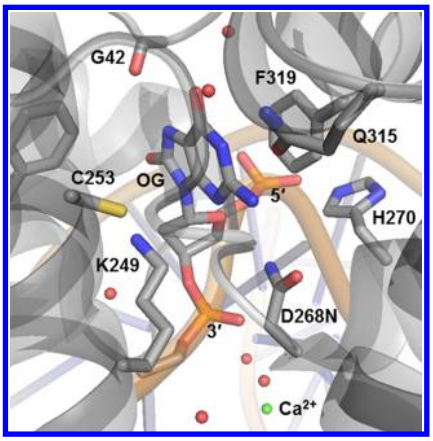

Figure 9. Important hOgg1 active-site residues identified in the crystal structure of the D268N mutant (PDB ID: 1N3C).[17]

lesions. First, the positive charge accumulating on Nε throughout the deglycosylation reaction could be stabilized by the catalytically important Asp268.[17,23] This can result from electrostatic stabilization due to the proximity of the anionic (aspartate) and cationic (cross-link) charges.[17] Alternatively, Asp268 or a water molecule could partially or fully abstract a proton from Lys249 through a hydrogen bond with the terminal amine during the deglycosylation step to generate a neutral cross-linked intermediate. Second, the OG leaving group could be stabilized through protonation by or hydrogen bonding with active-site residues. Previous computational investigations have protonated N3 or O8 of 8-oxoguanine through transfer from Lys prior to deglycosylation,[27,29,30] which lowers the deglycosylation barrier. Furthermore, water molecules present near O6 of OG in most crystal structures[13,16−19,21,23] could stabilize the departing base through hydrogen-bond donation. Indeed, a single water molecule bound to O6 can increase the N9 acidity of OG (a measure of leaving group ability) by 10.3 kJ mol^{-1}.[52] In addition, Gln315, which is near O6/N1 of OG, has been shown to modestly affect catalysis and therefore may fulfill this role.[20,24] These hydrogen-bonding interactions may be unnecessary, however, as a recent experimental study found nonpolar analogues of OG with little or no hydrogen-bonding accepting ability to be substrates of hOgg1.[25,26] Third, the free nucleobase product could be stabilized by nonspecific interactions with active-site residues. For example, a cationic histidine residue (His270, Figure 9) is in close proximity to the 5′-phosphate, and one of the proposed roles of this amino acid is stabilization of the negative charge accumulating on the nucleobase.[24] Although a stacking interaction between OG and Phe319 could contribute to catalysis, recent work shows that stacking has little to no effect on the deglycosylation barrier of deoxyuridine,[53] and thus, a catalytic contribution from the Phe319 residue is unlikely. From the above discussion, one can see that there are a multitude of possible catalytic approaches that hOgg1 can use to reduce the inherently large deglycosylation barrier.

Ring-Opening. In the present work, two different ring-opening pathways were characterized that involve either direct or base (OG$^-$) assisted proton transfer from Nε to O4′. As expected, assisted transfer is significantly more favorable than direct transfer (by more than 70 kJ mol^{-1}, Table 2). However, direct transfer leads to a beneficial orientation of the 4′-hydroxyl group that lowers the subsequent elimination barriers. Therefore, the ideal enzymatic mechanism will use a general base positioned on the opposite side of the sugar plane opposite to the nucleobase. This location will allow interactions between the 4′-hydroxyl and 3′-phosphate groups without requiring rotation of the hydroxyl group by 180°, which would inevitably cleave strong hydrogen bonds between the 4′-hydroxyl and general base. Depending on the orientation of the sugar moiety and nearby water molecules in the active site, this role could be fulfilled by Asp268 in hOgg1. This new proposal is consistent with evidence that this helix-capping residue is involved in multiple steps.[17,23] In addition, the efficient proton transfer between a Schiff base and an aspartate residue has been observed in bacteriorhodopsin.[54]

A second point of mechanistic flexibility investigated in this manuscript is the effect of transferring the *pro*−*R* versus the *pro*−*S* Nε proton. When the *pro*−*S* proton is transferred, the remaining N−H bond is directed toward the 3′-phosphate in the intermediate. In the subsequent elimination phase, the cationic Nε−H···O$_P$ hydrogen bond provides substantial stabilization to the leaving group. Furthermore, the *pro*−*S* hydrogen is aligned for transfer after nucleophilic attack by lysine at the anomeric carbon (IC(a), Figure 3), and therefore, less rearrangement is required for transfer of Nε−H$_S$ to O4′ than transfer of Nε−H$_R$. The reduced motion increases the probability that the ring-opening phase catalyzed by hOgg1 (or other bifunctional glycosylases) involves Nε−H$_S$ transfer, since the peptide backbone constrains the orientation of the lysine side chain (or other amine-containing nucleophile). Combined, these features indicate that transfer of Nε−H$_S$ is preferable to transfer of Nε−H$_R$ during enzyme-catalyzed ring-opening.

β-Elimination. Eight mechanistic variations of the β-elimination of the 3′-phosphate group (with abstraction of a C2′−H) were characterized in the present study (Table 1). The mechanisms differ in the C2′-proton abstracted (C2′−H$_S$ or C2′−H$_R$), the initial conformation of the imine linkage (*E* or *Z*), and the presence (or absence) of an O4′−H···N9 hydrogen bond. Reaction potential energy surfaces generated for two systems (D-N$_S$C$_S$ and A-N$_R$C$_R$) clearly demonstrate a favored asynchronous (E1) mechanism (Figure 8). In general, *pro*−*S* abstraction is lower in energy than *pro*−*R* abstraction, consistent with the C2′−H$_S$ hydrogen requiring less molecular motion/flexibility in order to interact with OG. The D/A-N$_R$C$_R$ mechanisms are an exception and exhibit the lowest abstraction and O3′-dissociation barriers (Table 2). Despite large structural differences, all elimination mechanisms exhibit similar energetics. These results are consistent with experiments showing

both *pro*−*R* and *pro*−*S* proton abstraction.[16] Another noteworthy feature of the *β*-elimination step is that the O3′-dissociation barrier is larger than the C2′−H abstraction barrier is (by 20−90 kJ mol^{-1}). Computational studies of similar reactions have conversely found that proton abstraction is rate-limiting,[32,33] likely due to the absence of cationic charge adjacent to the proton abstraction site in those systems.

Although the elimination barriers are lower than those for deglycosylation (and direct ring-opening), the barriers are quite large (up to 123.0 kJ mol^{-1}, Table 2). Therefore, it is useful to consider possible ways that enzymes might catalyze this reaction step. The most obvious mode of catalysis in hOgg1 involves stabilization of the phosphate leaving group. Examination of the hOgg1 active site (Figure 9) reveals a nearby calcium dication that could interact with the cleaved product upon displacement of a bound water molecule. Alternatively, since the phosphate group is accessible to solvent, proton transfer from solvent to the phosphate may distribute the charge. Finally, the proton transfer from N*ε* observed in the D-N_SC_R, A-N_RC_R, and A-$N_{R/S}C_S$ mechanisms (Figures 5 and 7) could reduce the charge on the 3′-phosphate moiety and prepare the protein−DNA linkage for hydrolysis and enzyme regeneration. A more subtle route for enzyme catalysis involves steric constraints that may promote rotation of the sugar−lysine linkage to better align a particular C2′−H for abstraction. In fact, modeling of crystal structures of the hOgg1-linked intermediate indicates rotation about C2′−C3′ leads to a lower energy geometry with C2′−H_R in close proximity to the OG nucleobase,[16] which promotes *pro*−*R* proton abstraction by the base.

Monofunctional Activity. There is some debate in the literature regarding the relevance of the hOgg1 lyase activity *in vivo*, since interactions with APE1 (EC#: 4.2.99.18) dissociate hOgg1 from the AP-site before elimination occurs.[23,25,55−57] Our results (Figure 2) provide the first computational support for the monofunctional activity of hOgg1. Specifically, the lowest energy point on the potential energy surface occurs during the ring-opening step, after the (N*ε*) amine has been deprotonated but before the deoxyribose ring has opened (Figure 2). If the protein−DNA cross-link is hydrolyzed at this point, the product would be an AP-site that can be processed by a more efficient AP-endonuclease (for example, APE1). Alternatively, a water molecule (potentially activated by a hydrogen bond to an active-site residue) could act as the nucleophile for the glycosylase step, and thus avoid the slow, multistep enzyme regeneration pathway. Recent work indicates that an aspartate-activated water nucleophile lowers the deglycosylation barrier of the dOG nucleotide by ∼20 kJ mol^{-1} compared to a lysine nucleophile (e.g., hOgg1) or ∼10 kJ mol^{-1} compared to a proline nucleophile (e.g., FPG) in a protein environment (ε = 4.2).[31] This new proposal of a water nucleophile would additionally bypass the confusion surrounding the mechanism for Lys249 activation in hOgg1.[15,17,23,29]

Since the sugar moiety of the damaged nucleoside is solvent accessible in most (if not all) DNA glycosylases, it is reasonable to propose a mechanism of action for hOgg1 that is monofunctional in nature by either of the aforementioned mechanisms. Parallels can be drawn to adenine−DNA glycosylase (MutY), which contains the same active-site motif as hOgg1 comprised of a helix-hairpin-helix element followed by a glycine/proline-rich loop ending in an invariant aspartate residue (HhH-GPD).[3,4] This monofunctional glycosylase uses a water nucleophile to catalyze deglycosylation of dA incorrectly incorporated opposite dOG.[58] A single mutation that incorporates lysine into the active site, equivalent to Lys249 in hOgg1, bestows bifunctional activity upon MutY.[37] Furthermore, some studies have even observed Schiff-base intermediates with wild-type protein, suggesting MutY exhibits weak, uncoupled lyase activity.[59−65] Thus, through comparison to the structurally similar MutY, one can envision a mechanism whereby the glycosylase and lyase activities of hOgg1 are uncoupled and the AP-site may be transferred to an AP-endonuclease for further processing. Indeed, there is evidence that hOgg1 glycosylase activity is increased and lyase activity is uncoupled in the presence of human AP-endonuclease (HAP1).[56] A similar argument can be made for endonuclease III, since it contains the same active-site fold as hOgg1 and MutY,[66] and therefore may correspondingly exhibit uncoupled monofunctional activity that is not limited by slow lyase activity.

CONCLUSIONS

For the first time, the lyase step of a bifunctional glycosylase has been modeled. Our results emphasize that computational approaches that include small models can provide several key conclusions regarding this complicated process through analysis of multiple reaction mechanisms. With respect to the first phase of the chemical step, our results clearly show that the protein must significantly lower the deglycosylation barrier. Catalysis will likely involve stabilization of both the nucleobase leaving group and the cationic charge developing on the protein−DNA cross-link. In the second phase, the most efficient rearrangement to a ring-opened Schiff base intermediate involves catalysis by a general base in the active site. Transfer of the *pro*−*S* proton on N*ε* in the cross-link during ring-opening requires less rotation about the C1′−N*ε* bond, exhibits lower barriers, and leads to more stable intermediates during the elimination phase than *pro*−*R* transfer. Once the ring has opened, the cross-link is very flexible and can occupy many different conformations throughout the remainder of the mechanism. Therefore, as long as the phosphate leaving group is stabilized (for example, through active-site contacts), the similar energetics for the different elimination pathways suggests that there is no intrinsic preference for a given mechanism, and the preferred mechanism may instead be dictated by steric constraints within the active site. Perhaps most interestingly, the lowest energy structure along the various pathways occurs *before* the *β*-elimination phase, which implies that it may be possible to kinetically trap this (deglycosylated, ring-closed) intermediate. This finding provides the first computational support for the recent experimental observation that hOgg1 exhibits monofunctional activity *in vivo*,[23] and by analogy supports the uncoupled lyase behavior of MutY.[37] This intricate feature of the reaction pathway underscores the complex mechanisms of action available to the DNA glycosylase family.

Large model studies of hOgg1 using the mechanistic insights outlined herein are currently underway in our group. Specifically, the present work indicates that mechanisms involving both *pro*−*S* and *pro*−*R* abstraction from C2′ during *β*-elimination must be considered since *pro*−*S* abstraction is slightly energetically favored, but *pro*−*R* abstraction leads to more facile O3′-elimination. Furthermore, most mechanisms characterized herein can likely be accommodated in the hOgg1 active site if the general acid/base role of OG in the small model is fulfilled by other residues (for example, an aspartate

residue), and careful consideration of the active-site composition will aid identification of the subset of reactions that must be considered. Such large-scale modeling of hOgg1 may further clarify the roles of active-site residues proposed to be important for the catalytic activity of hOgg1 based on this small model study (for example, Asp268, His270, and Gln315, Figure 9).[24] Although our group is particularly interested in hOgg1, our results regarding the flexibility of the imine linkage may be applied equally well to other enzymes with β-lyase activity on an AP-site, such as endonuclease III (hNTH in humans), endonuclease VIII (hNEIL in humans), MutY (hMYH in humans), and FPG, as well as model peptides. Equivalent large model studies of these enzymes may reveal structural causes for the observed relative rates. Mechanisms that obey the steric constraints in the active site of a given enzyme can be selected for additional study by overlaying our DFT elimination products (with the OG nucleobase removed) onto the desired active site, and fulfilling the catalytic role(s) of OG in our small model by other groups as needed. Studies of such a diverse group of lyase-active enzymes will no doubt reveal additional mechanistic insights into this vital reaction.

■ ASSOCIATED CONTENT

Supporting Information

Energetics on B3LYP/6-31+G(d) geometries, coordinates of all structures, and the full citation for ref 49. This material is available free of charge via the Internet at http://pubs.acs.org.

■ AUTHOR INFORMATION

Corresponding Author

*E-mail: stacey.wetmore@uleth.ca.

Notes

The authors declare no competing financial interest.

■ ACKNOWLEDGMENTS

Financial support was provided by the Natural Sciences and Engineering Council of Canada (NSERC), the Canada Research Chair program, and the Canada Foundation for Innovation (CFI). Computer resources were provided by the Upscale and Robust Abacus for Chemistry in Lethbridge (URACIL) and WestGrid, part of the Compute/Calcul Canada HPC platform. J.L.K. thanks NSERC (CGS-D) and the University of Lethbridge for graduate student scholarships.

■ REFERENCES

(1) Hitomi, K.; Iwai, S.; Tainer, J. A. *DNA Repair* **2007**, *6*, 410−428.
(2) Sun, B.; Latham, K. A.; Dodson, M. L.; Lloyd, R. S. *J. Biol. Chem.* **1995**, *270*, 19501−19508.
(3) Stivers, J. T.; Jiang, Y. L. *Chem. Rev.* **2003**, *103*, 2729−2759.
(4) Berti, P. J.; McCann, J. A. B. *Chem. Rev.* **2006**, *106*, 506−555.
(5) Kuznetsov, N. A.; Koval, V. V.; Fedorova, O. S. *Biochemistry (Moscow)* **2011**, *76*, 118−130.
(6) Sakai, A.; Nakanishi, M.; Yoshiyama, K.; Maki, H. *Genes Cells* **2006**, *11*, 767−778.
(7) Fujimoto, H.; Pinak, M.; Nemoto, T.; Bunta, J. K. *Cent. Eur. J. Phys.* **2007**, *5*, 49−61.
(8) McCulloch, S. D.; Kokoska, R. J.; Garg, P.; Burgers, P. M.; Kunkel, T. A. *Nucleic Acids Res.* **2009**, *37*, 2830−2840.
(9) Cadet, J.; Douki, T.; Ravanat, J.-L. *Free Radical Biol. Med.* **2010**, *49*, 9−21.
(10) Kanvah, S.; Joseph, J.; Schuster, G. B.; Barnett, R. N.; Cleveland, C. L.; Landman, U. *Acc. Chem. Res.* **2010**, *43*, 280−287.
(11) van Loon, B.; Markkanen, E.; Hübscher, U. *DNA Repair* **2010**, *9*, 604−616.
(12) Nash, H. M.; Lu, R. Z.; Lane, W. S.; Verdine, G. L. *Chem. Biol.* **1997**, *4*, 693−702.
(13) Bruner, S. D.; Norman, D. P. G.; Verdine, G. L. *Nature (London, U.K.)* **2000**, *403*, 859−866.
(14) Norman, D. P. G.; Bruner, S. D.; Verdine, G. L. *J. Am. Chem. Soc.* **2001**, *123*, 359−360.
(15) Bjoras, M.; Seeberg, E.; Luna, L.; Pearl, L. H.; Barrett, T. E. *J. Mol. Biol.* **2002**, *317*, 171−177.
(16) Fromme, J. C.; Bruner, S. D.; Yang, W.; Karplus, M.; Verdine, G. L. *Nat. Struct. Biol.* **2003**, *10*, 204−211.
(17) Norman, D. P. G.; Chung, S. J.; Verdine, G. L. *Biochemistry* **2003**, *42*, 1564−1572.
(18) Chung, S. J.; Verdine, G. L. *Chem. Biol.* **2004**, *11*, 1643−1649.
(19) Banerjee, A.; Yang, W.; Karplus, M.; Verdine, G. L. *Nature (London, U.K.)* **2005**, *434*, 612−618.
(20) Banerjee, A.; Verdine, G. L. *Proc. Natl. Acad. Sci. U.S.A.* **2006**, *103*, 15020−15025.
(21) Radom, C. T.; Banerjee, A.; Verdine, G. L. *J. Biol. Chem.* **2007**, *282*, 9182−9194.
(22) Lee, S.; Radom, C. T.; Verdine, G. L. *J. Am. Chem. Soc.* **2008**, *130*, 7784−7785.
(23) Dalhus, B.; Forsbring, M.; Helle, I. H.; Vik, E. S.; Forstrøm, R. J.; Backe, P. H.; Alseth, I.; Bjørås, M. *Structure (Cambridge, MA, U.S.)* **2011**, *19*, 117−127.
(24) van der Kemp, P. A.; Charbonnier, J. B.; Audebert, M.; Boiteux, S. *Nucleic Acids Res.* **2004**, *32*, 570−578.
(25) Zharkov, D. O.; Rosenquist, T. A.; Gerchman, S. E.; Grollman, A. P. *J. Biol. Chem.* **2000**, *275*, 28607−28617.
(26) McKibbin, P. L.; Kobori, A.; Taniguchi, Y.; Kool, E. T.; David, S. S. *J. Am. Chem. Soc.* **2012**, *134*, 1653−1661.
(27) Osakabe, T.; Fujii, Y.; Hata, M.; Tsuda, M.; Neya, S.; Hoshino, T. *Chem-Bio Inf. J.* **2004**, *4*, 73−92.
(28) Schyman, P.; Danielsson, J.; Pinak, M.; Laaksonen, A. *J. Phys. Chem. A* **2005**, *109*, 1713−1719.
(29) Calvaresi, M.; Bottoni, A.; Garavelli, M. *J. Phys. Chem. B* **2007**, *111*, 6557−6570.
(30) Zheng, Y.; Xue, Y.; Yan, S. G. *THEOCHEM* **2008**, *860*, 52−57.
(31) Shim, E. J.; Przybylski, J. L.; Wetmore, S. D. *J. Phys. Chem. B* **2010**, *114*, 2319−2326.
(32) Kim, Y.; Mohrig, J. R.; Truhlar, D. G. *J. Am. Chem. Soc.* **2010**, *132*, 11071−11082.
(33) Pei, Q.; Christofferson, A.; Zhang, H.; Chai, J. J.; Huang, N. *Biophys. Chem.* **2011**, *157*, 16−23.
(34) de Jesus, K. P.; Serre, L.; Zelwer, C.; Castaing, B. *Nucleic Acids Res.* **2005**, *33*, 5936−5944.
(35) Mazumder, A.; Gerlt, J. A.; Absalon, M. J.; Stubbe, J.; Cunningham, R. P.; Withka, J.; Bolton, P. H. *Biochemistry* **1991**, *30*, 1119−1126.
(36) Zharkov, D. O.; Golan, G.; Gilboa, R.; Fernandes, A. S.; Gerchman, S. E.; Kycia, J. H.; Rieger, R. A.; Grollman, A. P.; Shoham, G. *EMBO J.* **2002**, *21*, 789−800.
(37) Williams, S. D.; David, S. S. *Nucleic Acids Res.* **1998**, *26*, 5123−5133.
(38) Kurtz, A. J.; Dodson, M. L.; Lloyd, R. S. *Biochemistry* **2002**, *41*, 7054−7064.
(39) Rogacheva, M. V.; Kuznetsova, S. A. *Russ. Chem. Rev.* **2008**, *77*, 765−788.
(40) Dong, J.; Drohat, A. C.; Stivers, J. T.; Pankiewicz, K. W.; Carey, P. R. *Biochemistry* **2000**, *39*, 13241−13250.
(41) Scharer, O. D.; Jiricny, J. *Bioessays* **2001**, *23*, 270−281.
(42) Millen, A. L.; Manderville, R. A.; Wetmore, S. D. *J. Phys. Chem. B* **2010**, *114*, 4373−4382.
(43) Churchill, C. D. M.; Wetmore, S. D. *Phys. Chem. Chem. Phys.* **2011**, *13*, 16373−16383.
(44) Schroeder, G. K.; Wolfenden, R. *Biochemistry* **2007**, *46*, 13638−13647.
(45) Scalmani, G.; Frisch, M. J. *J. Chem. Phys.* **2010**, *132*, 114110.
(46) Ng, J. A.; Vora, T.; Krishnamurthy, V.; Chung, S. H. *Eur. Biophys. J. Biophys. Lett.* **2008**, *37*, 213−222.

(47) Zhao, Y.; Truhlar, D. G. *J. Chem. Theory Comput.* **2010**, *6*, 1104−1108.
(48) Ribeiro, R. F.; Marenich, A. V.; Cramer, C. J.; Truhlar, D. G. *J. Phys. Chem. B* **2011**, *115*, 14556−14562.
(49) Frisch, M. J.; Truck, G. W.; Schlegel, H. B.; Scuseria, G. E.; Robb, M. A.; Cheeseman, J. R.; Scalmani, G.; Barone, V.; Mennucci, B.; Petersson, G. A.; et al. *Gaussian 09*, revision A.1; Gaussian, Inc.: Wallingford, CT, 2009.
(50) Bjoras, M.; Luna, L.; Johnson, B.; Hoff, E.; Haug, T.; Rognes, T.; Seeberg, E. *EMBO J.* **1997**, *16*, 6314−6322.
(51) Brinkmeyer, M. K.; Pope, M. A.; David, S. S. *Chem. Biol.* **2012**, *19*, 276−286.
(52) McConnell, T. L.; Wheaton, C. A.; Hunter, K. C.; Wetmore, S. D. *J. Phys. Chem. A* **2005**, *109*, 6351−6362.
(53) Kellie, J. L.; Navarro-Whyte, L.; Carvey, M. T.; Wetmore, S. D. *J. Phys. Chem. B* **2012**, *116*, 2622−2632.
(54) Sato, Y.; Hata, M.; Neya, S.; Hoshino, T. *J. Phys. Chem. B* **2006**, *110*, 22804−22812.
(55) Hill, J. W.; Hazra, T. K.; Izumi, T.; Mitra, S. *Nucleic Acids Res.* **2001**, *29*, 430−438.
(56) Vidal, A. E.; Hickson, I. D.; Boiteux, S.; Radicella, J. P. *Nucleic Acids Res.* **2001**, *29*, 1285−1292.
(57) Morland, I.; Luna, L.; Gustad, E.; Seeberg, E.; Bjoras, M. *DNA Repair* **2005**, *4*, 381−387.
(58) McCann, J. A. B.; Berti, P. J. *J. Am. Chem. Soc.* **2008**, *130*, 5789−5797.
(59) Tsai-wu, J. J.; Liu, H. F.; Lu, A. L. *Proc. Natl. Acad. Sci. U.S.A.* **1992**, *89*, 8779−8783.
(60) Lu, A. L.; Tsaiwu, J. J.; Cillo, J. *J. Biol. Chem.* **1995**, *270*, 23582−23588.
(61) Gogos, A.; Cillo, J.; Clarke, N. D.; Lu, A. L. *Biochemistry* **1996**, *35*, 16665−16671.
(62) Manuel, R. C.; Lloyd, R. S. *Biochemistry* **1997**, *36*, 11140−11152.
(63) Guan, Y.; Manuel, R. C.; Arvai, A. S.; Parikh, S. S.; Mol, C. D.; Miller, J. H.; Lloyd, S.; Tainer, J. A. *Nat. Struct. Biol.* **1998**, *5*, 1058−1064.
(64) Zharkov, D. O.; Grollman, A. P. *Biochemistry* **1998**, *37*, 12384−12394.
(65) Williams, S. D.; David, S. S. *Biochemistry* **1999**, *38*, 15417−15424.
(66) Fromme, J. C.; Verdine, G. L. *EMBO J.* **2003**, *22*, 3461−3471.